

## Supplementary Information

### Nonlinear diffusion, bonding, and mechanics of the interface between austenitic steel and iron

Qin Qin <sup>a,\*</sup>, Wei He <sup>a</sup>, Lu Xie <sup>a</sup>, Junchao Deng <sup>a</sup>, Xuehui Zhu <sup>a</sup> and Qing Peng <sup>b,\*</sup>

a School of Mechanical Engineering, University of Science and Technology Beijing, Beijing 100083, China

b Nuclear Engineering and Radiological Sciences, University of Michigan, Ann Arbor, MI 48109, USA

\*Corresponding authors: [qinqin@me.ustb.edu.cn](mailto:qinqin@me.ustb.edu.cn). (Q.Q.) and [qpeng@umich.edu](mailto:qpeng@umich.edu) (Q.P.)

#### 1 MD model of Fe-Cr-Ni /Fe

Two kinds of alloys, 316L stainless steel and Q345R carbon steel were intentionally selected for the hot-compressing simulation due to their importance as structural materials in industry. As can be seen from Table S1, various kinds of elements (>9) are contained in 316L and Q345R, which leads to a great challenge in atomic modeling of 316L and Q345R. To overcome the difficulties, we only model those prominent components with concentration > 10 wt.%. The elements with low concentration in 316L and Q345R steels were in general believed to be less important of the interface morphology and ignored in this study. Therefore, Q345R steel was considered as pure Fe without any other elements, simple because the Fe is predominant with over 98 wt.%. The 316L stainless steel was simplified only containing Fe, Cr and Ni elements, where the mass fraction of Cr and Ni were 16.03% and 10.03%, respectively, as shown in Table S1. Combining the two parts forming the interface, we use the model of Fe-Cr-Ni/Fe for 316L/Q345R metal composite in this study.

**Table S1** Material Elements Composition

Materials	C	Si	Mn	P	S	Cr	Ni	Mo	Al	Ti
Q345R	0.17	0.27	1.40	0.011	0.007	0.023	0.02	<0.01	<0.01	<0.01
SUS316L	0.017	0.42	1.26	0.031	0.003	16.03	10.03	1.95		

## 2 Diffusion between interfaces

Fig. S1 shows the configurations after the compression loading at various temperature. As shown in Fig. S1, there is obvious interfacial diffusion between FeCrNi and Fe. The thicknesses of the diffusion layer can be obtained by extracting the coordinate information of the atoms from the LAMMPS dump files, where the diffusion layer is specified that both the atomic concentration of FeCrNi and Fe along the compression direction (direction Z) are more than 5%.

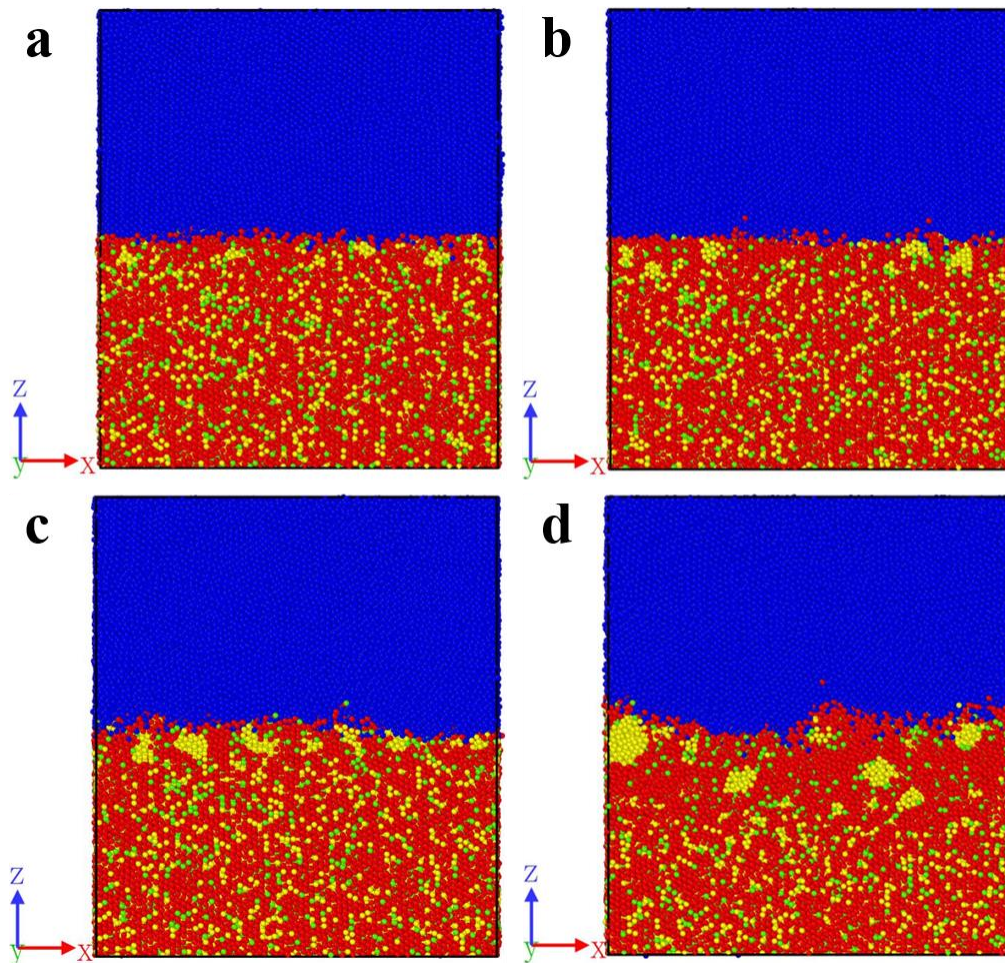


**Fig. S1** Snapshots of interfacial diffusion at a constant strain rate of  $3.0 \times 10^9 \text{ s}^{-1}$  with various temperatures after the compression loading, (a):1500 K, (b):1600 K, (c):1700 K, (d):1800 K. (The top layer is Fe, the bottom layer is FeCrNi; ● : Fe atom in the Fe, ● : Fe atom in the FeCrNi, ● : Cr atom in the FeCrNi, ● : Ni atom in the FeCrNi).

As shown in Fig. S2, the thicknesses of diffusion layer increases exponentially with temperature increase, where the thicknesses of diffusion layer is 6.5 Å, 8 Å, 12.5 Å and 18.5 Å when the temperature is 1500 K, 1600 K, 1700 K and 1800 K, respectively.

Therefore, the thickness of diffusion layer gets larger with temperature. This is a direct evidence that the growth of the layer is diffusion controlled which is greatly influenced by the temperature. As a result, it is more efficient to obtain a thicker diffusion layer and better interface combination when the composite temperature is higher.

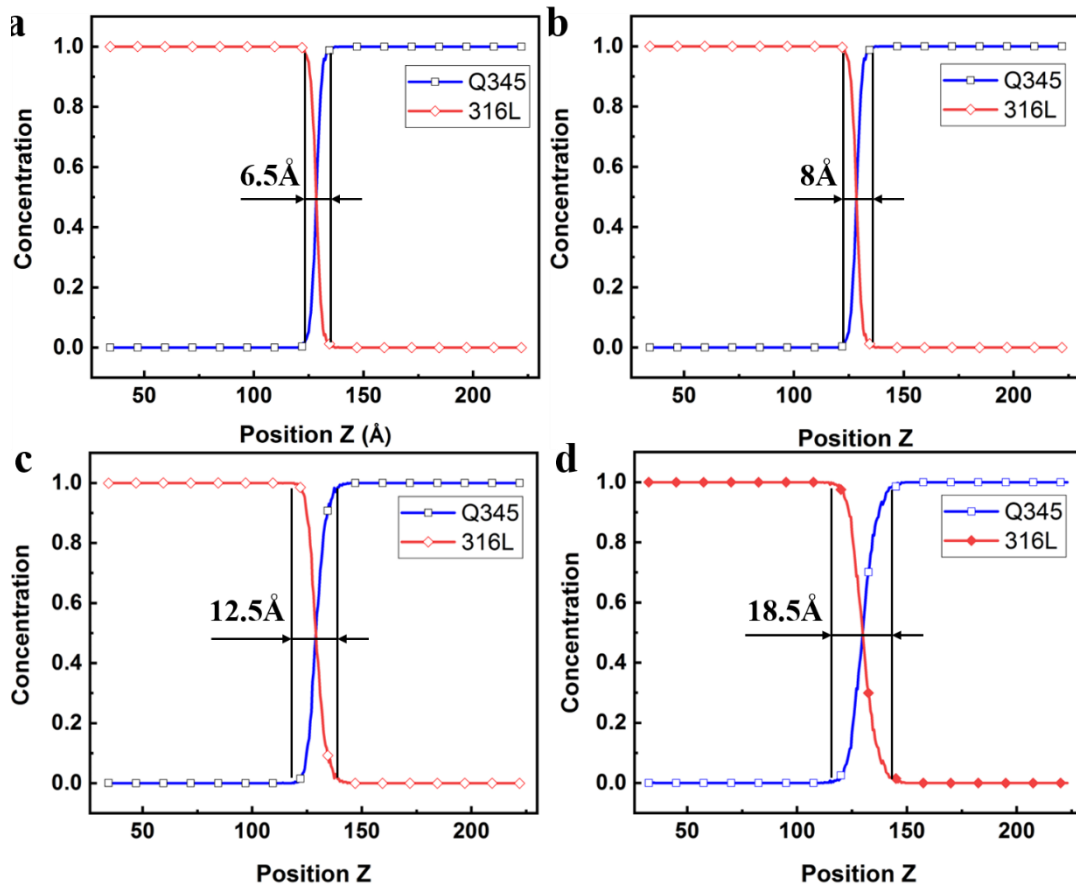
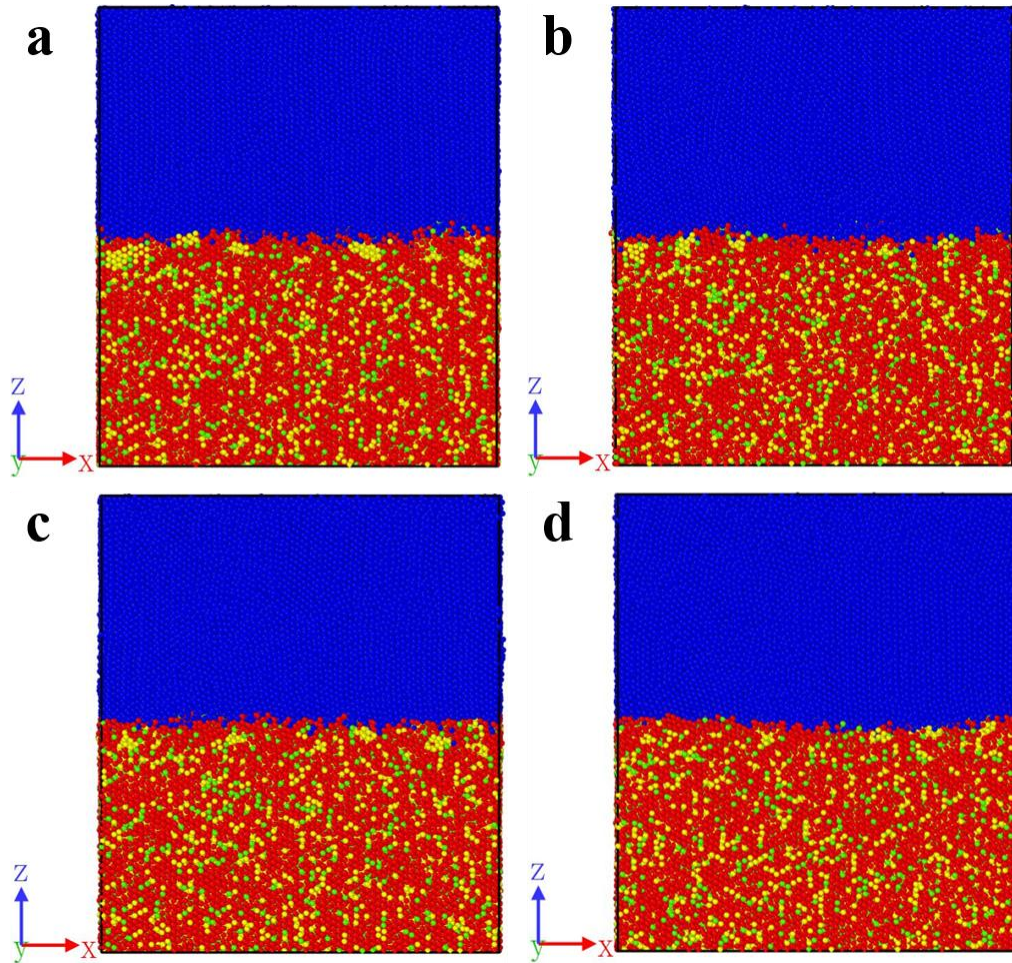


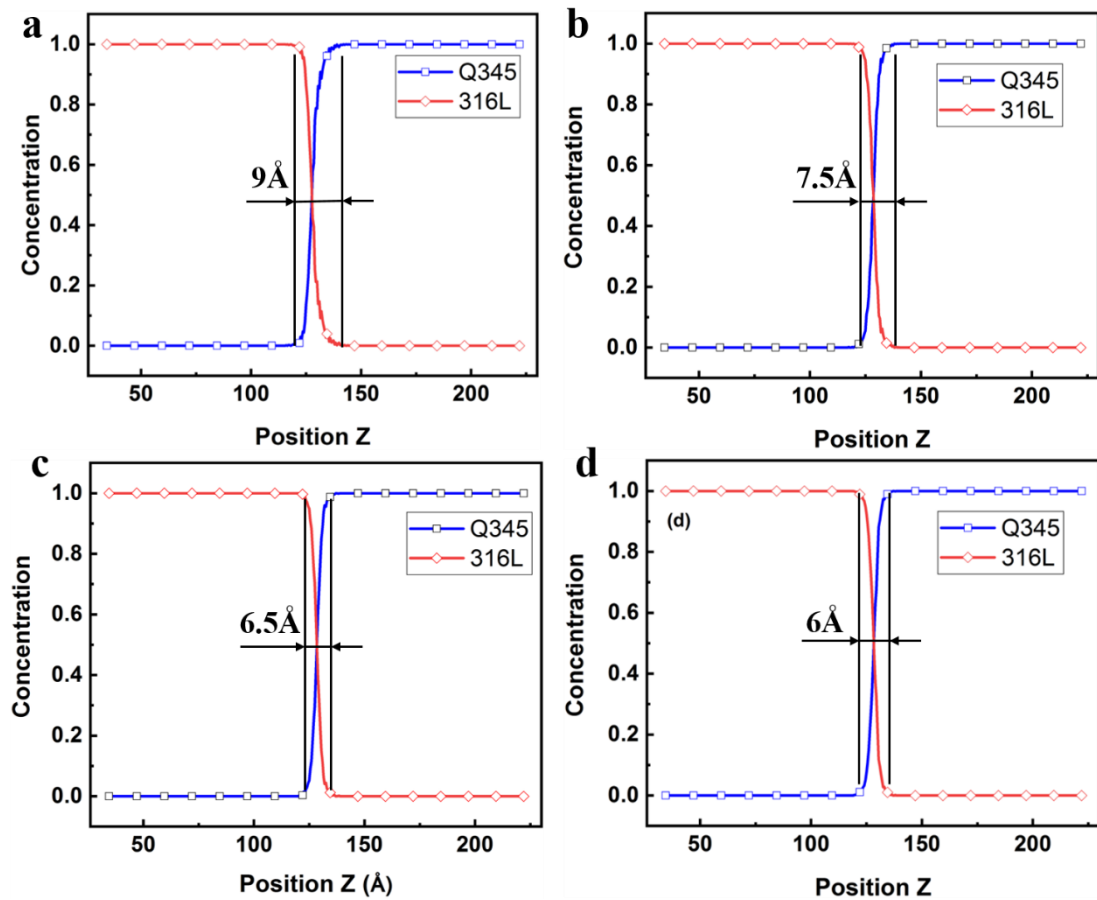
Fig. S2 Atomic concentration distribution of Position Z at a constant strain rate of  $3.0 \times 10^9 \text{ s}^{-1}$  with various temperatures after the compression loading, (a):1500 K, (b):1600 K, (c):1700 K, (d):1800 K.

Fig. S3 shows the configurations after the compression loading at various strain rate. As shown in Fig. S3, there is obvious interfacial diffusion between FeCrNi and Fe.



**Fig. S3** Snapshots of interfacial diffusion at a constant temperature of 1500 K with various strain rates after the compression loading, (a):  $1.0 \times 10^9 \text{ s}^{-1}$ , (b):  $1.5 \times 10^9 \text{ s}^{-1}$ , (c):  $3.0 \times 10^9 \text{ s}^{-1}$ , (d):  $4.0 \times 10^9 \text{ s}^{-1}$ .

As shown in Fig. S4, Similarly, the thickness of diffusion layer decreases exponentially with strain rate increase, which are  $9 \text{ \AA}$ ,  $7.5 \text{ \AA}$ ,  $6.5 \text{ \AA}$  and  $6 \text{ \AA}$  at  $1 \times 10^9 \text{ s}^{-1}$ ,  $1.5 \times 10^9 \text{ s}^{-1}$ ,  $3 \times 10^9 \text{ s}^{-1}$  and  $4 \times 10^9 \text{ s}^{-1}$ , respectively. Obviously, the thickness of the diffusion layer decreases as the strain rate increases, which reaches a drop of 33.3% when the strain rate increases from  $1 \times 10^9 \text{ s}^{-1}$  to  $4 \times 10^9 \text{ s}^{-1}$ . It can be explained that the compression time is inversely proportional to the strain rate on the premise of reaching the same strain 0.3. Therefore, it is necessary to select the appropriate compressive strain rate to obtain a thicker diffusion layer. We can conclude that the optimized condition is the hot compression with strain rate of  $3 \times 10^9 \text{ s}^{-1}$  when take both composite quality and simulation time into consideration.



**Fig. S4** Atomic concentration distribution of Position Z at a constant temperature of 1500 K with various strain rates after the compression loading, (a):  $1.0 \times 10^9 \text{ s}^{-1}$ , (b):  $1.5 \times 10^9 \text{ s}^{-1}$ , (c):  $3.0 \times 10^9 \text{ s}^{-1}$ , (d):  $4.0 \times 10^9 \text{ s}^{-1}$ .

### 3 The melting points of Fe and Fe<sub>74</sub>Cr<sub>16</sub>Ni<sub>10</sub>

To further make sure that this potential can afford the high-temperature study in this report, this potential has been used to measure the melting points of Fe and Fe<sub>74</sub>Cr<sub>16</sub>Ni<sub>10</sub>, respectively. First, the model of pure Fe was built with BCC crystal structure, which was put inside a simulation box with dimensions of 13.5(X) × 13.5(Y) × 13.5(Z) nm<sup>3</sup>. As shown in Fig. S5(a), there were 172773 atoms in this model. Second, the system was relaxed sufficiently to obtain an equilibrium state at 1300 K with isobaric–isothermal (NPT) ensemble. The velocity-Verlet algorithm was applied to integrate the motion equation for the atoms in the structure with a constant time step of  $1 \times 10^{-15}$  s. Finally, the temperature was increased from 1300 K to 2400 K. Fig. S5(b) showed the curve of total energy as a function of temperature. Total energy showed a linear increase when the temperature increased from 1300 K to 1868 K and increased rapidly at 1868 K, indicating that the melting points of Fe was 1868 K. Good agreement was obtained in comparison with experimental results (1811 K).

The process of measuring the melting points  $\text{Fe}_{74}\text{Cr}_{16}\text{Ni}_{10}$  was similar with that of Fe. As shown in Fig. S5(c), there were 182250 atoms in the model of  $\text{Fe}_{74}\text{Cr}_{16}\text{Ni}_{10}$ . Fig. S5(d) showed the curve of total energy as a function of temperature. Total energy showed a linear increase when the temperature increased from 1300 K to 2137 K and increased rapidly at 2137 K, indicating that the melting points of  $\text{Fe}_{74}\text{Cr}_{16}\text{Ni}_{10}$  was 2137 K. Good agreement was obtained in comparison with experimental results (2123 K). In conclusion, this potential can afford the high-temperature (1500 K-1800 K) study in this report.

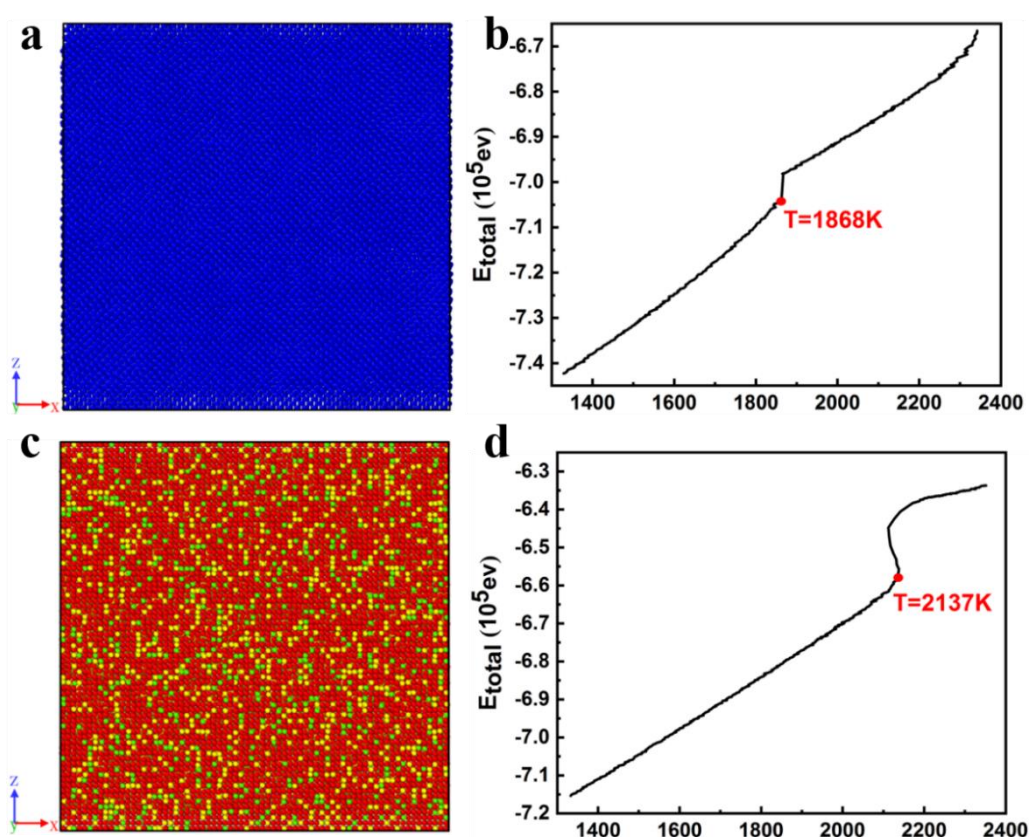


**Fig. S5** (a): Snapshot of Fe model after relaxation, (b): Total energy of the Fe model as a function of the temperature, (c): Snapshot of FeCrNi model after relaxation, (d): Total energy of the FeCrNi model as a function of the temperature.

#### 4 PRDFs for cFe-sFe, cFe-Ni and cFe-Cr

In order to clarify which kind of atoms of 316L were more likely to bonded to the Fe atoms in Q345 when 316L diffused to Q345, the diffusion layer was extracted. PRDFs for cFe-sFe, cFe-Ni and cFe-Cr for diffusion layer at the end of uniaxial compression have been analyzed. The larger the first peak of the PRDF graph, the

more the two atoms are combined. As showed in Fig. S6, the first peak of cFe-Ni was higher than that of cFe-Cr. Therefore, Ni atoms in 316L were more easily bonded to Fe atoms in Q345 than that of Cr atoms. Because the melting point of Cr is much higher than the melting point of Ni. The higher the melting point of the metal, the stronger the bonding force between the atoms, and the diffusion activation energy is proportional to the bonding force between the atoms.

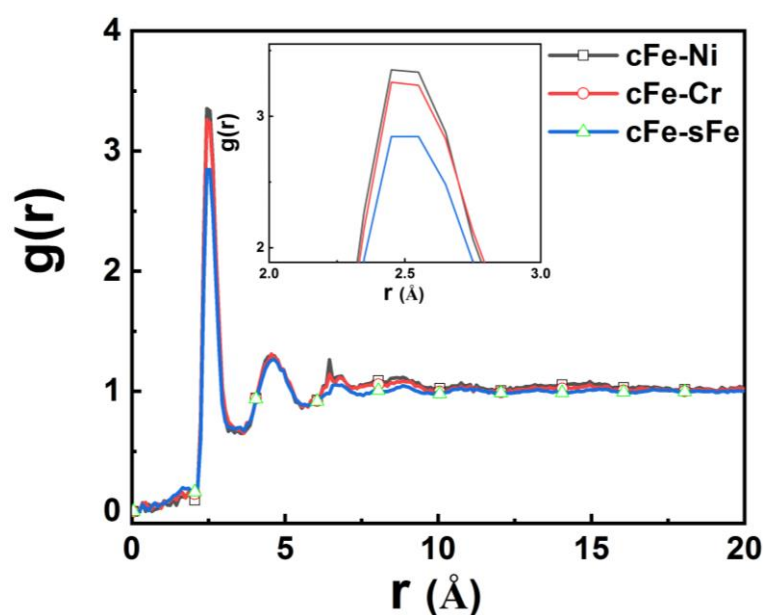


Fig. S6 PRDFs for cFe-sFe, cFe-Ni and cFe-Cr for diffusion layer at the end of uniaxial compression.

## 5 Experimental analysis

We have carried out an experimental analysis when studying the formation mechanism of oxide inclusions on the interface of stainless steel clad plates after hot rolled. The experimental materials were 316 stainless steel (composite) and Q345 low carbon steel (substrate). The size of 316 stainless steel was 300 mm × 300 mm × 10 mm, and the size of Q345 low carbon steel was 300 mm × 300 mm × 90 mm.

The experiment consisted of four steps. First, the surface of 316 and Q345 was machined to a certain roughness. Second, the surrounding area was welded and evacuated, and the degree of vacuum was 0.1 Pa. Third, the sealed composite slab was heated to 1473 K for 2 h and then rolled on a two-roll hot rolling mill. The rolling temperature was 1423 K and the finishing temperature was controlled between 1223

K and 1323 K. Finally, the hot-rolled sample was polished, and then the carbon steel layer was etched with 4% nitric acid. The microstructure of the interface was observed using a 200 MAT optical microscope produced by ZEISS and a Quanta 400 scanning electron microscope (SEM). And the distribution of elements such as Cr and Ni on the two sides of the composite interface were analyzed using an energy disperse (EDS, Energy Disperse Spectrum) produced by FEI.

As shown in Figure S7(a), the microscopic characteristics of the interface was observed using a 200 MAT optical microscope. The total reduction was 50% and a single pass was 5%. Obviously, the macro interface is not a straight line, but a slightly curved curve. Figure S7(b) showed the results of energy disperse spectrum of the interface. Obviously, many kinds of elements were found by EDS analysis such as O, Fe, Ni, Cr, Si, Mn, and Al. In addition to the Fe and Cr elements in the oxide, other elements also had a high mass fraction such as Si, Mn and Al. While Fe and Cr were intrinsic elements in steel, and other elements should reach the vicinity of the composite interface by diffusion from a position away from the interface at a high temperature. As shown in Fig. S7(c), the distribution of elements such as Cr and Ni on the two sides of the composite interface were analyzed by using EDS analysis. Obviously, Fe, Cr and Ni on both sides of the interface vary greatly. In stainless steel, Cr and Ni diffused through the original interface to carbon steel. The diffusion distance of Cr was about 10 $\mu$ m, and the diffusion distance of Ni was about 5 $\mu$ m. Because the concentration gradient of Cr on both sides of the interface was higher than that of Ni. Good agreement was obtained in comparison with simulation results.

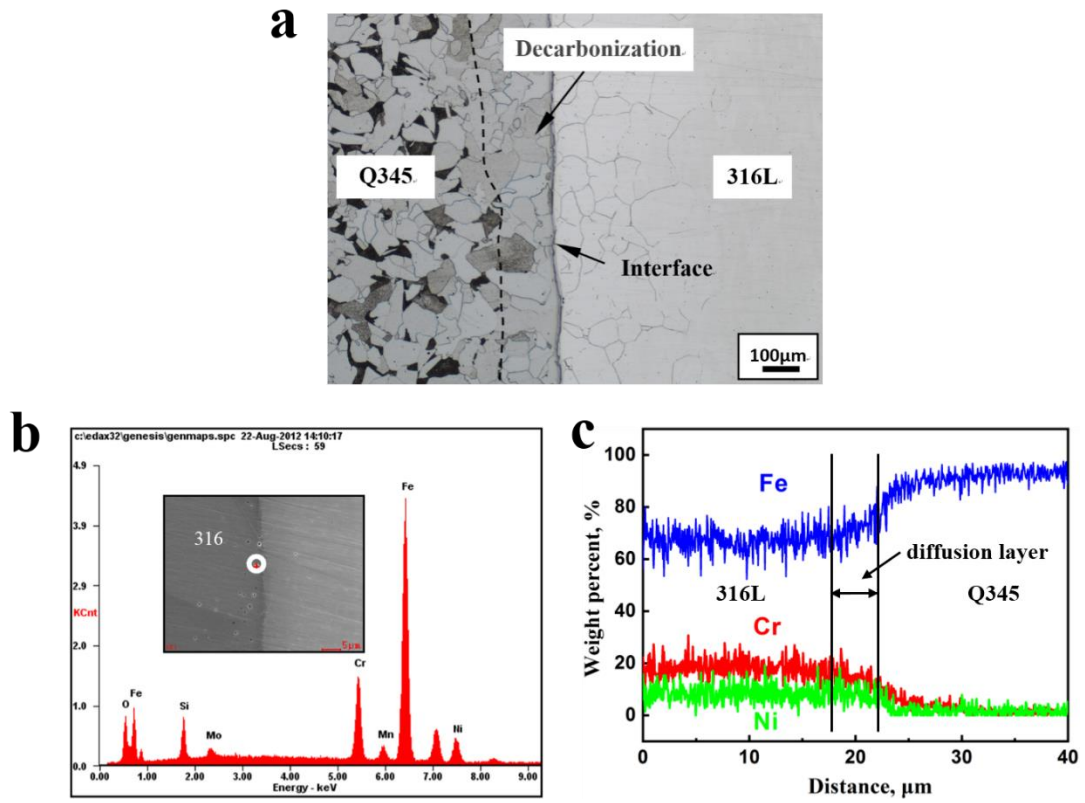


**Fig. S7** (a): the microscopic characteristics of the composite interface, (b): the results of energy disperse spectrum of the interface, (c): The distribution of elements such as Cr and Ni on the two sides of the composite interface.